J Mol Model (2008) 14:409–416
DOI 10.1007/s00894-008-0287-y

ORIGINAL PAPER

Characterization of a complete cycle of acetylcholinesterase catalysis by *ab initio* QM/MM modeling

Alexander V. Nemukhin · Sofia V. Lushchekina · Anastasia V. Bochenkova · Anna A. Golubeva · Sergei D. Varfolomeev

Received: 17 September 2007 / Accepted: 8 February 2008 / Published online: 15 March 2008

Abstract The reaction mechanism of acetylcholine hydrolysis by acetylcholinesterase, including both acylation and deacylation stages from the enzyme-substrate (ES) to the enzyme-product (EP) molecular complexes, is examined by using an *ab initio* type quantum mechanical – molecular mechanical (QM/MM) approach. The density functional theory PBE0/aug-6–31+G* method for a fairly large quantum part trapped inside the native protein environment, and the AMBER force field parameters in the molecular mechanical part are employed in computations. All reaction steps, including the formation of the first tetrahedral intermediate (TI1), the acylenzyme (EA) complex, the second tetrahedral intermediate (TI2), and the EP complex, are modeled at the same theoretical level. In agreement with the experimental rate constants, the estimated activation energy barrier of the deacylation stage is slightly higher than that for the acylation phase. The critical role of the non-triad Glu202 amino acid residue in orienting lytic water molecule and in stabilizing the second tetrahedral intermediate at the deacylation stage of the enzymatic process is demonstrated.

A. V. Nemukhin · S. V. Lushchekina · S. D. Varfolomeev
N.M. Emanuel Institute of Biochemical Physics,
Russian Academy of Sciences,
4 ul. Kosygina,
Moscow 119334, Russian Federation

A. V. Nemukhin (✉) · A. V. Bochenkova · A. A. Golubeva · S. D. Varfolomeev
Department of Chemistry,
M.V. Lomonosov Moscow State University,
1/3 Leninskie Gory,
Moscow 119991, Russian Federation
e-mail: anem@lcc.chem.msu.ru

Keywords Acetylcholinesterase · Acetylcholine hydrolysis · QM/MM modeling · Reaction mechanism

Introduction

Acetylcholinesterase (AChE) is a serine hydrolase which terminates impulse transduction at cholinergic brain synapses. It rapidly hydrolyses the neurotransmitter acetylcholine (ACh) shown in Scheme 1 to choline and acetic acid.

The significance of the AChE catalytic process is explained by the observation that the malfunctioning of this enzyme is related to serious human diseases. In particular, there are discovered factors that may contribute to the involvement of acetylcholine in Gulf War syndrome [1] and Alzheimer's disease [2]. Another important feature of AChE is that the enzyme hydrolyzes acetylcholine with a remarkably high rate showing about 13 orders of enhancement compared to aqueous solution [3].

Since 1991, when the first crystallographic structure of *Torpedo californica* acetylcholinesterase (TcAChE) was resolved, numerous structures of the enzyme were reported. Presently about 100 structures of AChEs from different species are available in the Protein Data Bank (PDB) [4], including the apo and modified structures of TcAChE, murine and human AChEs. The structures of mutants, of complexes with inhibitors, the structures with the nerve agent soman, and other natural and synthetic complexes with ligands and hydrolysis products, as well as of radiation damaged species are available for analysis. All these crystal structures of AChE show that the enzymatic active site is located near the bottom of the 20 Å deep narrow gorge which consists of a large number of aromatic residues. The active site consists of two main areas: an esteratic sub-site containing a catalytic functional unit similar to that of

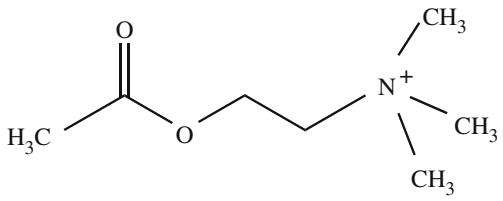

Scheme 1 Chemical structure of acetylcholine

serine hydrolase and serine protease families, and an anionic sub-site responsible for the binding of the positively charged tail group of ACh.

Conserved catalytic triad of human (for example, PDBID: 1F8U [5]) and mouse AChE consists of the Ser203, His447, and Glu334 amino acid residues. Mutation of any of these three residues by alanine causes loss of enzymatic activity [6]. The oxyanion hole, which is an important component of the active center, is formed by the peptidic NH groups from the Gly121, Gly122, and Ala204 side chains responsible for the hydrogen bonds with the carbonyl oxygen of the substrate. This is consistent with the crystallographic studies of AChE complexes with analogue substrates [7]. The importance of the Glu202 residue in the AChE catalysis was observed in a series of experimental kinetic studies of mutated enzymes [8, 9].

In the assumed reaction mechanism [10–12], the Ser203 and His447 residues are directly involved in the reaction, serving as nucleophilic attacking group and general acid-base catalytic elements, respectively, at the acylation stage of the enzymatic reaction. This stage proceeds in nucleophilic addition of oxygen from Ser203 to the carbonyl carbon of ACh initiated by the proton transfer from Ser203 to His447. The catalytic role of the third residue of the catalytic triad, here, Glu334, has been debated previously, however, the recent studies indicate that it plays a crucial role in stabilizing the first transition state through electrostatic interaction between the carboxylate of Glu334 and the incipient imidazolium cation [13–15]. Deacylation stage is expected to proceed in a similar way, assuming nucleophilic addition of the lytic water molecule to the carbonyl carbon of acylenzyme and a proton transfer to His447.

Modern molecular modeling tools including molecular docking, molecular dynamics (MD), quantum chemistry and the combined quantum mechanical – molecular mechanical (QM/MM) method provide valuable details in describing the enzymatic mechanism at the atomistic level. Series of simulations were performed in order to clarify the mechanism of substrate transport down the aromatic gorge [16–21]. As for modeling chemical transformations, the simulations by *Fuxreiter* and *Warshel* [14] for the acylation stage (from the enzyme-substrate to formation of the first tetrahedral intermediate) and by *Vagedes* and co-authors [22] for an initial part of the deacylation stage (from the acylenzyme to formation of the second tetrahedral intermediate) on the base of the empirical valence bond (EVB) theory [23] considered catalytic efficiency of AChE compared to the related reaction in water. The energetics of the reactions was explored by evaluation of activation free energies by using the EVB potential surface and a free energy perturbation approach [14, 22]. Semiempirical molecular orbital methods were employed for simulations of chemical transformations in the model molecular clusters mimicking active sites of AChE [24–26]. The Hartree-Fock/3–21G quantum chemistry method was used by *Wlodek* et al. [27] to estimate reaction energy diagrams of the first step in the acylation reaction for several simple models of the active site. Strongly simplified molecular cluster were also considered in [28, 29] for higher level quantum chemical calculations of the reaction energy profiles of the acylation step.

The use of the hybrid QM/MM method [30] allows one to compute the reaction energy profile for the active site atoms trapped inside the native protein environment. The recent papers [13, 31, 32] by *McCammon* and coauthors based on the *ab initio* type QM/MM method [33, 34] provided the mechanistic picture of the initial step of the acylation reaction in acetylcholinesterase catalysis from the enzyme-substrate complex to the first tetrahedral intermediate. In Ref. [13, 31] the authors considered two QM/MM partitioning schemes: the first utilized a smaller QM subsystem consisting of the substrate ACh and the side chains of Ser203 and His447, with a total of 44 QM atoms. In the second, larger QM subsystem also included the side chain of Glu334, leading to a total of 54 QM atoms. A geometry optimization procedure was applied to the QM/MM system with the HF/3–21G calculations in the quantum part. The MP2/6–31+G* method was used to recalculate potential energy barriers at the stationary points found in the HF/3–21G approximation resulting in the barrier heights 12.6 kcal mol^{-1} for the small QM subsystem and 10.5 kcal mol^{-1} for the large QM subsystem. The results obtained in these works underlined the role of particular amino acid residues in the vicinity of the active site in reactions of the wild type and mutated AChE at the acylation stage.

The aim of the present work is to examine the complete cycle of chemical transformations in the acetylcholine hydrolysis by AChE, including both acylation and deacylation stages, by analyzing the reaction energy profile computed at the uniform theoretical level. To this end we apply the advanced *ab initio* type QM/MM method with a large fragment of the reacting system included in the quantum part. The route from the enzyme-substrate (ES) to enzyme-product (EP) complexes through the acylenzyme (EA) and tetrahedral intermediates (TI1, TI2) considered

for the model system is kept the same for the entire reaction.

Methods

The initial structure of the enzyme-substrate complex was constructed following the crystallographic atomic coordinates taken from Protein Data Bank [4] for the E202Q mutant of AChE (PDBID:1F8U [5]). The side chain of Glu202 was restored, and hydrogen atoms were added with the help of the Reduce program [35]. Geometry optimization of added hydrogen atoms was performed by using the Tinker program [36] with the AMBER force field [37]. After removing the inhibitor, the ACh species was deposited in the active site by using the Autodock 3.0.4 program [38]. It should be noted that due to the small size of the ACh molecule its precise position inside the protein globule could only be accurately fitted with the help of the subsequent QM/MM geometry optimization. The cavities formed by the protein side-chains in the area of the active site and the gorge can contain water molecules that are crucial for enzyme functioning [19], which can be unresolved in the X-ray analysis. Therefore we performed a search of suitable cavities in the vicinity of the active site by using Tinker [36] and filled them with water molecules. The coordinates of all 137 water molecules introduced to the model system were optimized in MD simulations at temperatures of 300 K and 0 K with the AMBER force field [37].

We considered several approaches to partition the system to the quantum mechanical (QM) and molecular mechanical (MM) parts for QM/MM calculations. Apparently, those molecules and amino acid side chains which directly participate in the catalytic reaction or make a significant impact on the distribution of electron density in the active site should be included to the QM part. Therefore, the ACh moiety, three nearby water molecules, side chains of the catalytic triad Ser203, His447, Glu334, side chains of the oxianion hole residues Gly121, Gly122, Ala204, a fragment of Ser229 that forms hydrogen bond with Glu334 and influences the charge distribution in the system, as well as a side chain of Glu202, were included to the quantum subsystem. Figure 1 shows explicitly all 79 atoms in balls and sticks representation for which the energies and forces were computed by quantum chemical equations.

The rest of the model system was assigned to the MM part. Remote molecular groups located outside the active site (more distant than 8–10 Å) were spatially fixed at the crystal positions. Full QM/MM geometry optimization was performed for all other atoms. All QM/MM calculations were performed by using a version of the PC GAMESS computer program [39], specially adjusted for QM/MM modeling. In this program, the mechanical embedding QM/MM technique by *Bakowies* and *Thiel* [40] as implemented by *Kress* and *Granovsky* (http://classic.chem.msu.su/gran/gamess/index.html) was used.

The energy diagram for the reaction path for both acylation and deacylation steps, including the enzyme-substrate complex (ES), the acylenzyme complex (EA), the enzyme-product complex (EP), as well as the tetrahedral intermediates (TI1 and TI2) and the transition states (TS1 and TS2), was calculated in series of energy minimizations in the QM/MM approximation. The energy and forces were

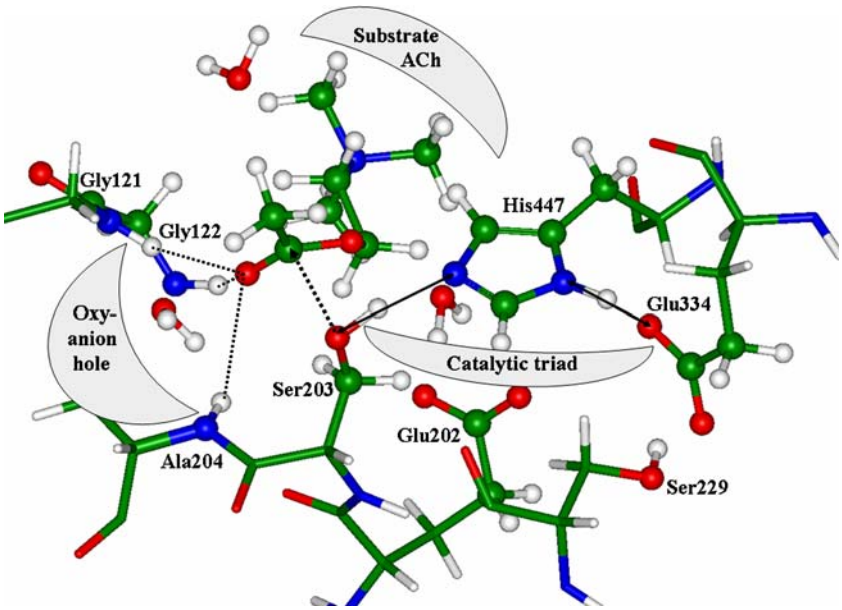

Fig. 1 The active site at the geometry of the enzyme-substrate complex. Balls and sticks distinguish the quantum subsystem. The catalytic triad comprises the residues Ser203, His447, Glu334. Oxyanion hole includes the residues Gly121, Gly122, Ala204. The dashed arrow illustrates the reaction coordinate for the acylation stage, i.e., nucleophilic addition of oxygen from Ser203 to the carbonyl carbon of ACh

computed by using the PBE0 exchange-correlation functional and the basis set 6–31+G* in the quantum part. Additional polarization functions were added to the hydrogen atoms, which participate in chemical transformations, and to the atoms of carboxyl groups of Glu334 and Glu202. The total amount of basis functions was 713. The AMBER force field parameters were used in the molecular mechanical part.

We report here the computed potential energy changes along the reaction coordinate, since direct calculations of entropic contributions and subsequent estimates of free energy changes are prohibitively expensive for such large model system. As shown, for instance, in recent calculations [32] of the potential energy path and corresponding free energy changes for the interactions of AChE with other substrates, potential energy and free energy profiles do not differ dramatically. Therefore, the conclusions drawn from the analysis of potential energy graphs should be correct enough.

Results

In simulations, we monitored carefully the hydrogen bond networks around the active site paying special attention to the following issues. (i) An interaction region of side chains of His447, Glu334 and Ser229. (ii) The hydrogen bonds between the carbonyl oxygen atom of substrate and the residues of oxyanion hole, Gly121, Gly122 and Ala204, that are responsible for proper orientation of the carbonyl group of substrate during the nucleophilic attack and stabilization of transition states and tetrahedral intermediates. (iii) The hydrogen bonds formed by the side chain of Glu202.

The structure of the enzyme-substrate complex is illustrated in Fig. 1. The initial step of the acylation reaction, from the ES-complex to the first tetrahedral intermediate, was characterized in several previous quantum-based simulations [13, 14, 24, 26–29, 31, 32]. Qualitatively, the features of this step were reproduced in our simulations. A natural choice of the reaction coordinate for this segment is clarified in Fig. 1 by showing with a dashed arrow the direction of nucleophilic attack of the Ser203 oxygen the carbonyl carbon of ACh. The residues of the oxyanion hole, Gly121, Gly122, and to a lesser extent, Ala204, form hydrogen bonds with the carbonyl oxygen of ACh and fix the position of its carbonyl carbon during the nucleophilic attack of O^{γ}_{Ser203}.

By gradually decreasing the initial $\left(O^{\gamma}_{Ser203} - C_{ACh}\right)$ distance, 2.48 Å, in the ES-complex and optimizing all other geometry coordinates in the model system we specified the minimum energy profile. At the transition state (TS1) geometry, the $\left(O^{\gamma}_{Ser203} - C_{ACh}\right)$ distance gets reduced to 2.16 Å. Evidences for the proton transfer from Ser203 to His447 were noticed by considering an elongation of the $\left(O^{\gamma}_{Ser203} - H^{\gamma}_{Ser203}\right)$ bond from 1.01 Å in ES to 1.17 Å in TS1, and a decrease of the $\left(H^{\gamma}_{Ser203} - N^{\varepsilon}_{His447}\right)$ distance from 1.71 Å in ES to 1.40 Å in TS1. Hydrogen bonds between the residues of the oxyanion hole, Gly121, Gly122, Ala204, and the carbonyl oxygen of ACh were getting shorter. The QM/MM energy of the TS1 structure was computed as 7.2 kcal mol^{-1} above the level of the ES complex.

Figure 2 illustrates the geometry configuration of the first tetrahedral intermediate (TI1) at the acylation stage. Its

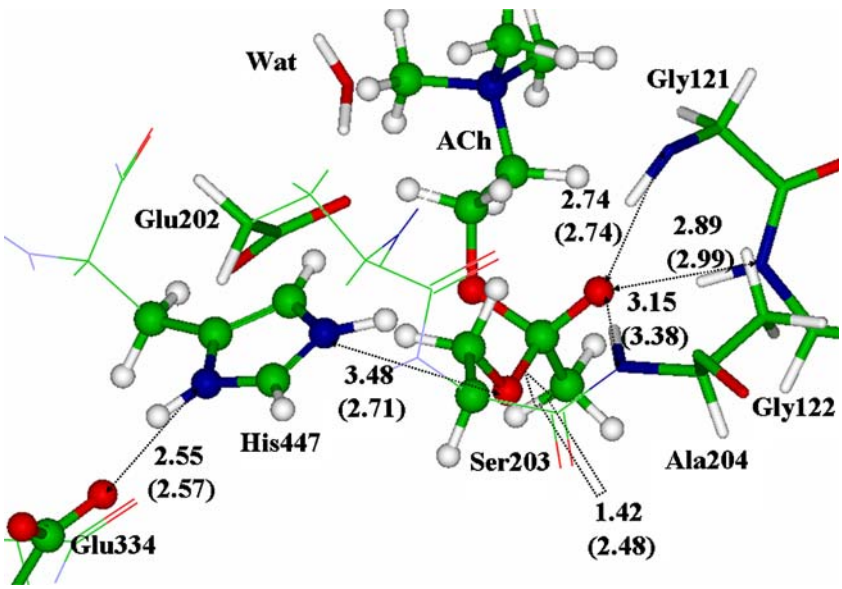

Fig. 2 Geometry configuration of the tetrahedral intermediate for the acylation step (TI1). The distances (in Å) without parentheses refer to TI1; the values in parentheses correspond to the ES-complex (Fig. 1)

energy is 12.5 kcal mol^{-1} lower that that of the ES-complex. The distance between the oxygen atom of Ser203 and carbon of ACh is now 1.42 Å corresponding to the formed covalent bond. Consistent with previous simulations [13, 14], we do not observe the proton transfer from His447 to the third member of the catalytic triad, Glu334.

The next step of the acylation reaction should lead to formation of the acylenzyme (EA) structure. Computationally, this was accomplished by moving the proton on N^{ε} of His447 to the esteratic oxygen of ACh and performing an unconstrained minimization of the QM/MM energy. As a result, the first tetrahedral intermediate TI1 decayed, and the choline molecule separated from its precursor. Geometry configuration of this stationary point is illustrated in Fig. 3 showing the choline molecule in yellow sticks. The QM/MM energy of this model system is of about 5 kcal mol^{-1} higher than that of TI1. We did not attempt to locate the transition state separating TI1 and EA, since according to the previous experience in modeling serine hydrolase reaction mechanism [41] its energy should be less than 4 kcal mol^{-1} above the TI1 level.

In the EA configuration, one of three water molecules assigned to the QM-part (labeled as Wat in Fig. 3) is apparently perfectly oriented by two hydrogen bonds with His447 and Glu202, for the subsequent attack of carbonyl C atom of acylenzyme. An initial value of the reaction coordinate for this step of the deacylation reaction, chosen as the (O_{Wat}-C_{AE}) distance, is 2.58 Å. By gradually decreasing this distance and optimizing all other geometry parameters of the model system we succeeded in locating the second transition state (TS2) and the second tetrahedral intermediate (TI2).

We performed a partial vibrational analysis at the located TS2 saddle point and analyzed the normal mode of single imaginary frequency, 800 i cm^{-1}. As expected, this mode corresponds primarily to the O-H_{Wat} stretch toward N^{ε} of His447 coupled to the O_{Wat}-C_{AE} stretching. The energy of the TS2 configuration is estimated as 8.4 kcal mol^{-1} with respect to the EA level and, therefore, in this approach, the activation barrier for the deacylation stage is higher than that for the acylation stage (7.2 kcal mol^{-1}).

Geometry configuration of the second tetrahedral intermediate TI2 is illustrated in Fig. 4. In this structure, the distance O_{Wat}-C_{AE} is 1.45 Å signifying formation of the covalent bond. Hydrogen from the lytic water molecule is transferred to His447, $R\left(H_{Wat} - N^{\varepsilon}_{His447}\right) = 1.04$ A. Oxianion hole residues Gly121 and Gly122 participate in hydrogen bonding with the carbonyl oxygen atom. Like at the acylation stage, no proton transfer occurs from His447 to the triad member Glu334. We pay special attention to the side chain of Glu202. Apparently it is an active member of the hydrogen bond network extending over the active site and participates in stabilization of TI2. The QM/MM energy of TI2 is lower than that of EA by 9.7 kcal mol^{-1}.

A proton transfer from His447 to acylenzyme, leading to the acetic acid, completes the catalytic cycle. We did not succeed in locating the corresponding transition state because of highly flat potential energy surface in this area. According to the energy scans the energy barrier separating TI2 and the enzyme-product complex (EP), if it occurs, should not exceed 1–2 kcal mol^{-1}.

The EP complex is shown in Fig. 5 in the same perspective as the ES starting point (Fig. 1). Apparently, the enzymatic active site is completely restored. In the presence of the

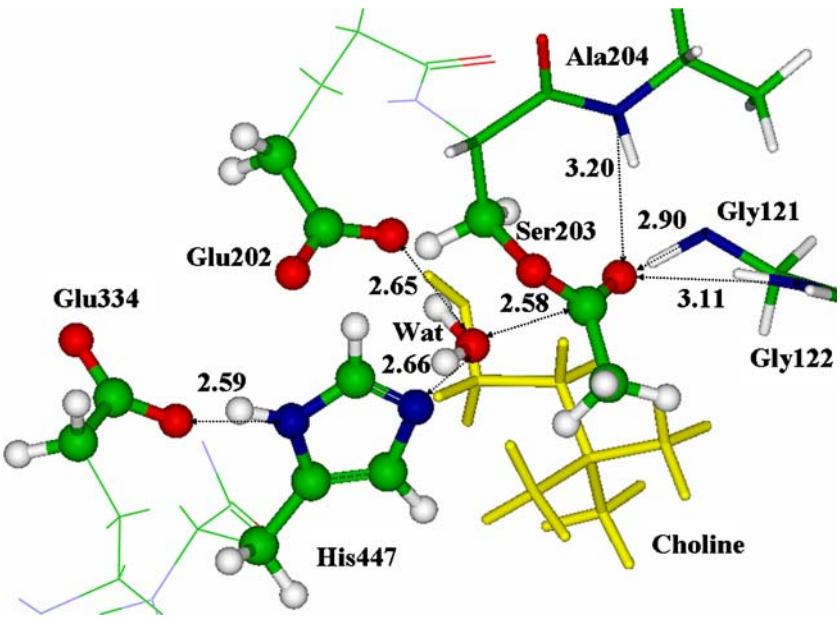

Fig. 3 Geometry configuration of the acylenzyme complex (EA). Distances between heavy atoms are given in angstroms. The choline molecule is shown in yellow sticks

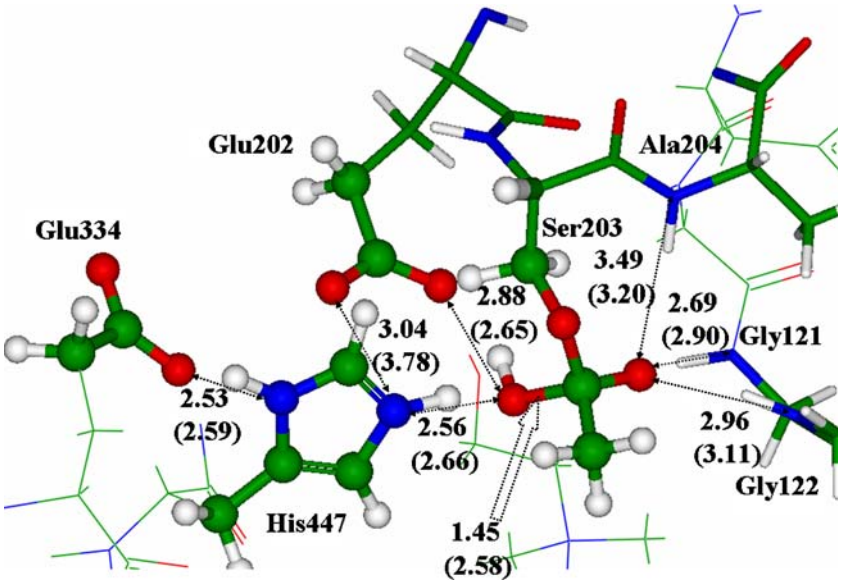

Fig. 4 Geometry configuration of the tetrahedral intermediate of deacylation stage (TI2). Values in parentheses refer to the EA complex (Fig. 3). Distances are given in angstroms

reaction products, choline and acetic acid, the QM/MM energy of the EP model system is 16.4 kcal mol^{-1} lower than that of the EA intermediate.

Figure 6 summarizes the entire computed QM/MM energy profile.

Discussion

Although several previous papers described the results of quantum-based calculations of separate steps of acetylcholinesterase catalysis [13, 14, 22, 24–29, 31, 32], the data obtained in this work for the entire cycle of chemical transformations in the active site provide substantial new knowledge on this important enzymatic process. Solid conclusions for the initial step of the acylation reaction proceeding from the enzyme-substrate complex to the first tetrahedral intermediate were summarized in [13, 31, 32] by the results of *ab initio* type QM/MM calculations.

We applied the *ab initio* type QM/MM theory with a larger fragment of the reacting site included to the QM-part (79 atoms) described at a higher quantum chemical level (PBE0/aug-6–31+G*) for analysis of the complete catalytic reaction including all steps of acylation and deacylation stages. Our computed pathway at the initial step of the acylation reaction qualitatively coincides with the results of previous QM/MM simulations [13, 31] despite the differences in starting enzyme-substrate models as well as in computational

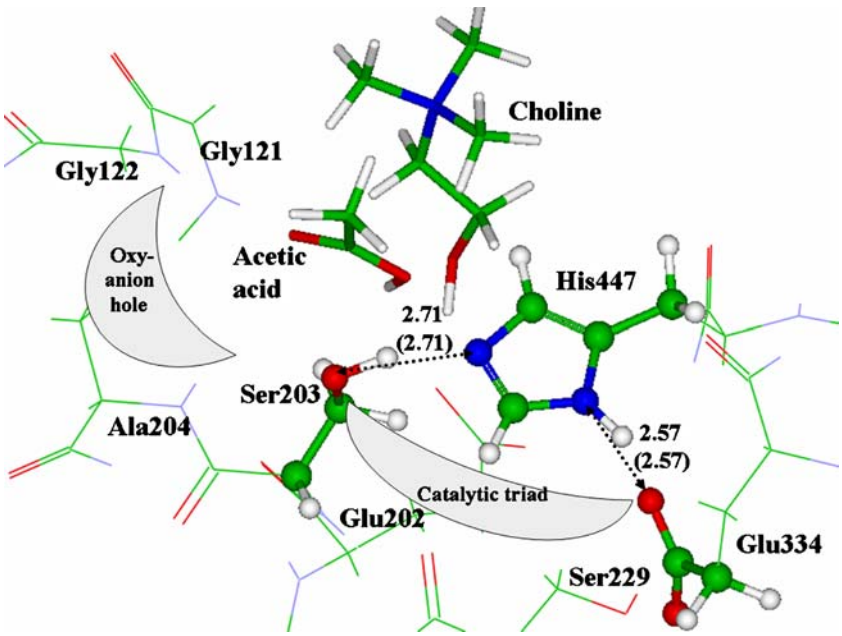

Fig. 5 Geometry configuration of the reaction products (EP). Distances (Å) without parentheses refer to EP, with parentheses – to ES (Fig. 1)

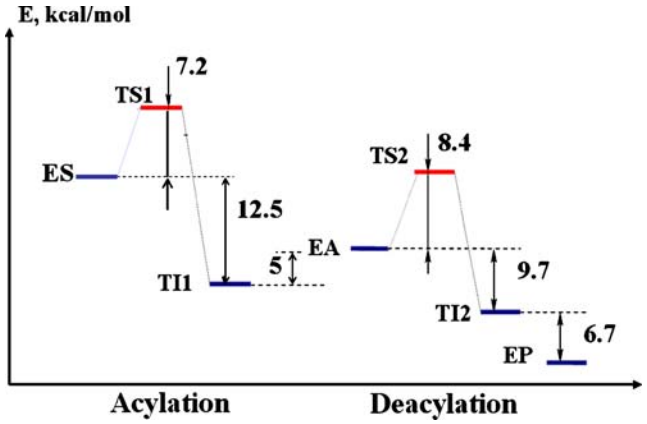

Fig. 6 The computed energy diagram for the reaction path from the enzyme – substrate complex (ES) to the enzyme-product complex (EP)

techniques. Taking into account that the MP2(6–31+G*)//HF (3–21G) method used in [13, 31] may overestimate the activation barrier, while the DFT methods used in our work (7.2 kcal mol^{-1}) usually underestimate the barrier heights [42], an agreement between these two approximations seems reasonable even at the quantitative level.

Our data completely agree with previous findings [13, 14] that the role of the third member of the catalytic triad, Glu334, cannot be associated with the so-called charge-relay or low-barrier hydrogen bond concepts. In both the acylation and deacylation stages the proton is localized on N^{δ} of His447 during the transformations. This conclusion is in line with the results of the previous QM/MM simulations of the serine protease catalytic mechanism with the Ser-His-Asp catalytic triad [43] or the serine carboxyl peptidases with the Ser-Glu-Asp triad [41].

What is a subject of debates is the role and the status of the amino acid residue Glu202 located in the immediate vicinity of the active site. Theoretical considerations of *Wlodek* et al. [27] stated that Glu202 should have a negative charge and removing this charge would result in a 32-fold reduction of the acylation rate. On the other hand, *Fuxreiter* and *Warshel* [14] found that the negative charge of Glu202 had only a moderate accelerating effect on the acylation stage. Also basing on the EVB calculations for the deacylation stage, *Vagedes* et al. [22] found that a negative charge at Glu202 increased the activation barrier from 14 to 20 kcal mol^{-1} in the absence of choline in the binding pocket. When considering available crystal structures of AChE we could not observe the structural patterns that benefit the neutral form of Glu202. Also, the results of QM/MM calculations favored the unprotonated (charged) state of this amino acid residue for all examined stationary points of the potential energy surface.

In summary, our data provide support to one of four hypotheses formulated in [13], namely, that "Glu202 might play an important role in the deacylation step". As clearly seen in Fig. 3 (EA), the side chain of the charged Glu202 is responsible for proper orientation of the lytic water molecule for the subsequent nucleophilic attack. As seen in Fig. 4 (TI2), Glu202 actively participates in hydrogen bond network including His447 and the second tetrahedral intermediate providing stabilization of the latter.

When discussing the computed energy values, especially for the activation barriers, we should consider possible sources of errors in the QM/MM procedure as well as in the modeling strategy applied in this work. According to the measurements for the hydrolysis reaction of [^{3}H]acetylcholine by AChE from *Electrophorus electricus* by *Froede* and *Wilson* [44], both acylation and deacylation stages may be considered as rate determining with the respective rate constants k_2 (1.7×10^6 min^{-1}) and k_3 (9.1×10^5 min^{-1}) as estimated from $k_{cat}=5.9\times10^5$ min^{-1}. Acylation is faster than deacylation, and therefore the activation energy barrier for the deacylation stage should be slightly higher, as obtained in our simulations.

As discussed above, the DFT quantum chemistry method, used in our QM part, usually underestimate the potential barriers and, most likely, the computed value for acylation (7.2 kcal mol^{-1}) is a lower bound to $\Delta E^{\#}$(acyl). The computed potential energy barrier for deacylation, $\Delta E^{\#}$(deacyl) ≈8.4 kcal mol^{-1}, should be corrected for the presence of choline in the reactive zone in simulations. We could not remove choline from the model system since it would violate a requirement of the uniform theoretical level for the entire catalytic cycle. Analysis of the model acylenzyme structure (Fig. 3) shows that the choline molecule is not involved in strong interactions with other groups in the active site, but nevertheless its presence may affect the computed value $\Delta E^{\#}$(deacyl), as well as the energy difference between the TI1 and EA stationary points.

We should also take into account that differences in entropic contributions to the free energy barriers, which actually correlate with the observed rate constants, may be substantial for the acylation and deacylation stages. Lastly, the mechanical embedding QM/MM scheme applied in the present work does not account for electronic polarization of the QM part, what introduces some errors in the calculated energy values.

Conclusions

This work presents the first effort to simulate the complete cycle of chemical transformations during the hydrolysis of acetylcholine in the active site of AChE from the enzyme-substrate (ES) to enzyme-product (EP) complexes by using a uniform computational approach and an invariable model system. For a large fraction of the reacting system involving 79 explicit QM atoms trapped inside the native protein

environment the energies and forces were computed at a high level DFT quantum chemistry level PBE0/aug-6–31+G*. Beyond ES and EP configurations, a series of stationary points on the potential energy surface, corresponding to the acylenzyme, tetrahedral intermediates at the acylation and deacylation stages as well as transition states separating the energy minima, were located.

Within our computational approach, we obtain that the activation energy for the deacylation stage is higher that that of the acylation stage what is qualitatively consistent with the experimental observation [44] that "acylation is faster than deacylation".

Also in agreement with experimental findings, our modeling demonstrates a critical role of the Glu202 amino acid residue. The unprotonated Glu202 species assists favorable orientation of the lytic water molecule and stabilization of the second tetrahedral intermediate at the deacylation stage of the process.

Acknowledgements This work was supported in part by the Russian Foundation for Basic Research (project # 07–03–00059) and by the Russian Academy of Sciences (program #10 of the Division of Chemistry and Materials). We thank A. Granovsky for generous help in calculations with the PC GAMESS package, and Dr. B. Grigorenko for valuable discussions on the paper.

References

1. Sapolsky RM (1998) Nature 393:306–309
2. Wright CI, Geula C, Mesulam MM (1993) Ann Neurol 34:373–384
3. Schowen RL (1978) In: Gandour RD, Schowen RL (eds) Transition states of biochemical processes. Plenum, New York, pp 77–114
4. Berman HM, Westbrook J, Feng Z, Gilliland G, Bhat TN, Weissig H, Shindyalov IN, Bourne PE (2000) Nucleic Acids Res 28:235–242
5. Kryger G, Harel M, Giles K, Toker L, Velan B, Lazar A, Kronman C, Barak D, Ariel N, Shafferman A, Silman I, Sussman JL (2000) Acta Crystallogr Sect D 56:1385–1394
6. Shafferman A, Kronman C, Flashner Y, Leitner M, Grosfeld H, Ordentlich A, Gozes Y, Cohen S, Ariel N, Barak D (1992) J Biol Chem 267:17640–17648
7. Harel H, Quinn DM, Nair HK, Sussman JL, Silman I (1996) J Am Chem Soc 118:2340–2346
8. Radic Z, Gibney G, Kawamoto S, MacPhee-Quigley K, Bongiorno C, Taylor P (1992) Biochemistry 31:9760–9767
9. Radic Z, Kirchhoff PD, Quinn DM, McCammon JA, Taylor P (1997) J Biol Chem 272:23265–23277
10. Rosenberry TL (1975) Adv Enzymol Relat Areas Mol Biol 43:103–218
11. Quinn DM (1987) Chem Rev 87:955–979
12. Tougu V (2001) Curr Med Chem 1:155–170
13. Zhang Y, Kua J, McCammon JA (2002) J Am Chem Soc 124:10572–10577
14. Fuxreiter M, Warshel A (1998) J Am Chem Soc 120:183–194
15. Warshel A, Naray-Szabo G, Sussman F, Hwang J-K (1989) Biochemistry 28:3629–3637
16. Gilson MK, Straatsma TP, McCammon JA, Ripoll DR, Faerman CH, Axelsen PH, Silman I, Sussman JL (1994) Science 263:1276–1278
17. Felder CE, Botti SA, Lifson S, Silman I, Sussman JL (1997) J Molec Graphics Model 15:318–327
18. Henchman RH, Tai K, Shen T, McCammon JA (2002) Biophys J 82:2671–2682
19. Kua J, Zhang Y, McCammon JA (2002) J Am Chem Soc 124:8260–8267
20. Bui JM, Henchman RH, McCammon JA (2003) Biophys J 85:2267–2272
21. Cheng Y, Suen JK, Radic Z, Bond SD, Holst MJ, McCammon JA (2007) Biophys Chem 27:129–139
22. Vagedes P, Rabenstein B, Åqvist J, Marelius J, Knapp E-W (2000) J Am Chem Soc 122:12254–12262
23. Warshel A (1991) Computer modeling of chemical reactions in enzymes and in solutions. Wiley, New York
24. Wang QM, Jiang HL, Chen JZ, Chen KX, Ji RY (1998) Int J Quant Chem 70:515–525
25. Wang QM, Jiang HL, Chen KX, Ji RY, Ye Y-J (1999) Int J Quant Chem 74:315–325
26. Sant'Anna CMR, Dos Santos Viana A, Do Nascimento NM (2006) Bioorg Chem 34:77–89
27. Wlodek ST, Antosiewicz J, Briggs JM (1997) J Am Chem Soc 119:8159–8165
28. Tachikawa H, Igarashi M, Nishihira J, Ishibashi T (2005) J Photochem Photobiol 79:11–23
29. Manojkumar TK Cui C, Kim KS (2005) J Comp Chem 26:606–611
30. Warshel A, Levitt M (1976) J Mol Biol 103:227–249
31. Zhang Y, Kua J, McCammon JA (2003) J Phys Chem B 107:4459–4463
32. Cheng YH, Cheng XL, Radic Z, McCammon JA (2007) J Am Chem Soc 129:6562–6570
33. Zhang Y, Lee T, Yang W (1999) J Chem Phys 110:46–54
34. Zhang Y, Liu H, Yang W (2000) J Chem Phys 112:3483–3492
35. Word JM, Lovell SC, LaBean TH, Taylor HC, Zalis ME, Presley BK, Richardson JS, Richardson DC (1999) J Mol Biol 285:1711–1733
36. Ponder JW (1999) TINKER: Software Tools for Molecular Design, Version 3.7. Washington University, St. Louis
37. Wang J, Wolf RM, Caldwell JW, Kollman PA, Case DA (2004) J Comp Chem 25:1157–1174
38. Morris GM, Goodsell DS, Halliday RS, Huey R, Hart WE, Belew RK, Olson AJ (1998) J Comput Chem 19:1639–1662
39. Nemukhin AV, Grigorenko BL, Granovsky AA (2004) Moscow Univ Chem Bull 59:1–28
40. Bakowies D, Thiel W (1996) J Phys Chem 100:10580–10594
41. Bravaya KB, Bochenkova AV, Grigorenko BL, Topol IA, Burt S, Nemukhin AV (2006) J Chem Theor Comput 2:1168–1175
42. Zhao Y, Gonzales-Garcia N, Truhlar DG (2005) J Phys Chem A 109:2012–2018
43. Nemukhin AV, Grigorenko BL, Rogov AV, Topol IA, Burt SK (2004) Theor Chem Acc 111:36–48
44. Froede HC, Wilson IB (1984) J Biol Chem 259:11010–11013